

Published in final edited form as:

Nat Neurosci. 2008 June ; 11(6): 631–633. doi:10.1038/nn.2120.

Red-shifted optogenetic excitation: a tool for fast neural control derived from *Volvox carteri*

Feng Zhang¹, Matthias Prigge², Florent Beyrière², Satoshi P Tsunoda², Joanna Mattis¹, Ofer Yizhar¹, Peter Hegemann², and Karl Deisseroth¹

¹ Departments of Bioengineering and Psychiatry, W083 Clark Center, 318 Campus Drive, Stanford University, Stanford, California 94305, USA

² Institute of Biology, Experimental Biophysics, Humboldt-University, Invalidenstraße 42, D-10115 Berlin, Germany

Abstract

The introduction of two microbial opsin-based tools, channelrhodopsin-2 (ChR2) and halorhodopsin (NpHR), to neuroscience has generated interest in fast, multimodal, cell type-specific neural circuit control. Here we describe a cation-conducting channelrhodopsin (VChR1) from *Volvox carteri* that can drive spiking at 589 nm, with excitation maximum red-shifted ~70 nm compared with ChR2. These results demonstrate fast photostimulation with yellow light, thereby defining a functionally distinct third category of microbial rhodopsin proteins.

Microbial proteins that can be rapidly activated by light have been adapted for research in neuroscience, including ChR2 and NpHR, which permit millisecond-precision optical control of genetically defined cell types in intact neural tissue^{1–6}. Because ChR2 is a blue light-gated cation channel and NpHR is a yellow light-driven chloride pump, the combination of these two proteins allows independent neural excitation and inhibition in the same preparation. However, there has been enormous interest in developing a hypothetical third major optogenetic tool, namely a second cation channel with an action spectrum that is substantially red-shifted relative to ChR2, to allow tests of the interaction of cell types in circuit computation or behavior.

Although efforts to develop a distinct light-activated excitatory protein have been focused on molecular engineering of ChR2, another approach would be to identify previously unknown microbial channelrhodopsins using genomic tools. One ChR2-related sequence from the spheroidal alga *Volvox carteri* (Fig. 1a) has been described, but the absorption spectrum of the protein and the photocycle dynamics are virtually identical to those of ChR2 (refs. 7,8). Therefore, we searched the genome database from the US Department of Energy Joint Genome Institute, discovered a second *Volvox* ChR (VChR1) that is more related to ChR1 (ref. 9) from *Chlamydomonas reinhardtii*, explored its properties in heterologous expression systems and functionally tested the codon-optimized opsin gene in mammalian neurons.

We expressed VChR1 in *Xenopus* oocytes and HEK293 cells and observed evoked photocurrents similar to those of ChR1 from *Chlamydomonas*^{9,10}. The photocurrents were graded with light intensity and showed inactivation from a fast peak toward a reduced stationary plateau (Fig. 1b). The peak preferentially appeared at high light intensities as a result of

Correspondence should be addressed to P.H. (E-mail: hegemap@rz.hu-berlin.de) or K.D. (E-mail: deissero@stanford.edu). Reprints and permissions information is available online at <http://npg.nature.com/reprints> and permissions

Note: Supplementary information is available on the Nature Neuroscience website.

accumulation of an expected late, nonconducting photocycle intermediate (Fig. 1b)⁹, and currents showed an inwardly rectifying current-voltage relationship (Fig. 1c).

Certain primary structural differences between VChR1 and the *Chlamydomonas* ChRs suggested that the properties of VChR1 would be distinct from those of the other ChRs (Fig. 1d). On the basis of electrostatic potential and quantum mechanical–molecular mechanical calculations for bacteriorhodopsin and relatives, the counterion complex of the all-*trans* retinal Schiff base (RSB; Fig. 1d) should be critical for color tuning^{11,12}, but these residues are conserved in both ChR1 and VChR1 (blue sequence, Fig. 1d). On the other hand, calculations and mutational experiments^{11,12} predict that four residues of the RSB binding pocket can contribute to absorption differences (red sequence, Fig. 1d); the first three are expected to be located near the RSB β -ionone ring (red structure, Fig. 1d), whereas the fourth is probably adjacent to the protonated nitrogen of the RSB (green structure, Fig. 1d). Notably, the β -ionone ring end of the RSB in VChR1 is expected to be more polar than that in ChR1 and ChR2, as positions 181 and 183 have been substituted with a polar Ser, whereas, conversely, the RSB nitrogen environment is less polar (S526A). The combination of these exchanges led us to expect a redistribution of positive charge along the RSB polyene system and a substantial red-shift compared with ChR2. Finally, one out of three other amino acids (green sequence, Fig. 1d) that are expected to modulate RSB charge distribution by long-range coupling is exchanged in both VChR1 and ChR1 (H114N). The 495-nm absorbance maximum of ChR1 (which does not express well in neurons) is indeed slightly red-shifted from that of ChR2 (ref. 9), but the combination of several substantial changes in VChR1 predicted a robust wavelength shift on a scale that would be useful for defining a new class of tool for neuroscience.

Although VChR1 did not appear to differ from ChR2 in ion selectivity under physiological conditions (conducting chiefly Na^+ , but also H^+ , K^+ and Ca^{2+} ; Fig. 1e), its wavelength dependence was indeed altered. VChR1-expressing oocytes were excited using 10-ns laser flashes across a range of wavelengths, allowing us to delineate a markedly red-shifted action spectrum, which revealed a maximum at ~ 535 nm and a small shoulder at lower wavelengths (Fig. 1f). To test the function of VChR1 in neurons, we constructed a lentivirus carrying the αCaMKII promoter to drive strong protein expression. To visualize VChR1 expression, we fused the seven transmembrane domains of VChR1 (residues 1–300; GenBank accession number EU622855) in frame to the amino terminus of yellow fluorescent protein (VChR1-EYFP). Neurons expressing VChR1-EYFP showed fluorescence similar to that reported previously for ChR2-EYFP (Fig. 2a), with the level of expression being slightly weaker than that of ChR2-EYFP using the same vector. Nevertheless, VChR1-EYFP neurons showed strong photocurrents when illuminated with 531-nm or 589-nm light (Fig. 2b). When the neurons were illuminated with 15 mW mm^{-2} of 531-nm light or 13.8 mW mm^{-2} of 589-nm light, the mean whole-cell inward currents were 208.8 ± 22.3 ($n = 20$; data are expressed as mean \pm s.e.m. unless otherwise stated) and 177.6 ± 24.7 pA ($n = 10$), respectively (Fig. 2c). The apparent time constants for the rise of the photocurrent were faster close to the wavelength of maximum activation as a result of the shift in absorption coefficient, with corresponding values of $\tau_{531_{\text{on}}} = 2.8 \pm 0.3$ ms and $\tau_{589_{\text{on}}} = 8.0 \pm 0.7$ ms ($n = 11$ for 531 nm and $n = 10$ for 589 nm). The corresponding decay time constants were $\tau_{531_{\text{off}}} = 133.4 \pm 11.7$ ms ($n = 11$) and $\tau_{589_{\text{off}}} = 135.7 \pm 9.8$ ms ($n = 10$).

We next explored the frequency dependence of VChR1 in driving spiking, using trains of 20 5-ms light pulses at 531 or 589 nm that were delivered to neurons in current clamp (exemplar traces from 589-nm excitation are shown in Fig. 2d). At up to 10 Hz, more than 90% of tested cells fired 100% of the action potentials in the train at either wavelength, and cells typically fired in response to $\sim 65\%$ of the light pulses at 20 Hz (Fig. 2e). In these strongly expressing cells, reliable spiking could be driven up to 30 Hz (Fig. 2d; pyramidal neurons in culture typically cannot follow 50 Hz or beyond in response to either current injection or ChR2

photostimulation), and doublets of spikes were occasionally evoked for a single light pulse at 531 nm, probably because the VChR1 τ_{off} decay constant was slower (133 ms) than that of ChR2 (12 ms). As with ChR2, VChR1 could also trigger excitatory postsynaptic potential–like subthreshold depolarizations with lower stimulation light intensities. Delivery of light-pulse barrages evoked typical summation of the subthreshold membrane voltage changes, with increasing light-pulse frequencies delivering increased steady-state depolarization (Fig. 2f).

To test for possible effects on membrane integrity, we compared the membrane resistances and resting membrane potentials (Fig. 2g,h) by whole-cell patch clamp of VChR1-EYFP–expressing neurons, nontransduced neurons and VChR1-EYFP–expressing neurons that were first patch clamped 24 h after exposure to a typical light-pulse protocol (1 s of 20 Hz per 5 ms light flashes, once per minute, for 10 min). The three groups had comparable recorded values ($P > 0.05$ for all comparisons), suggesting that VChR1-EYFP expression did not significantly alter membrane electrical properties⁴. Subcellular distribution was similar to that of ChR2. VChR1 was well tolerated and no all-*trans* retinal supplementation was needed in neurons.

Finally, we tested whether the pronounced spectral separation between ChR2 and VChR1 activation would be sufficient to enable separable activation. On the basis of our action spectra (Fig. 1f), we selected 589 and 406 nm as optimal excitation wavelengths with which to probe separable activation of ChR2 and VChR1. For neurons expressing either ChR2 or VChR1, we tested for evoked action potentials in response to trains of 20 5-ms light pulses delivered at 5 Hz. We also tested each wavelength at several different light intensities to determine the parameters that maximize ChR2, while minimizing VChR1, activation at 406 nm and vice versa. Indeed, we found that ChR2 and VChR1 neurons could be separated at 589 nm (Fig. 3a). In fact, no ChR2 neurons fired action potentials when illuminated with 589-nm light pulses of any intensity, as the absorption is effectively zero at this wavelength, whereas VChR1 neurons fired reliably at this wavelength. Conversely, all ChR2 neurons fired with 100% fidelity when illuminated with 406-nm light, at all three light intensities ($n = 7$; Fig. 3b). Although VChR1 cells were capable of firing occasional spikes in response to 406-nm flashes (all rhodopsins show some absorption at this wavelength), the percentage of spikes could be reduced to $13 \pm 9\%$, but not eliminated when the 406-nm light intensity was reduced to 1.2 mW mm^{-2} ($n = 10$; Fig. 3c), an intensity which continued to reliably drive spiking in the ChR2 neurons (Supplementary Methods online).

As currently implemented, the simultaneous application of VChR1 and ChR2 could be used to test the role of progressive recruitment of different cell populations in controlling circuit behavior. For example, two different local circuit populations could be progressively recruited in stepwise fashion by isolating population A with yellow light and then driving the combination of populations A and B with added blue light.

For other kinds of experiments it may be useful to drive two completely isolated populations at different times in the same preparation. At yellow wavelengths, the VChR1-labeled population will be exclusively controlled, whereas the contribution of the ChR2-labeled population will become steadily more dominant as the excitation wavelength becomes progressively bluer beyond 535 nm (Fig. 1f). However, overlap at the blue end of the spectrum presents a major challenge for *in vivo* experiments where a broad range of light intensities are present as a result of light scattering² and where it will therefore not be reliable to use light power–density tuning (Fig. 3) to improve spectral separation at short wavelengths. Looking toward the future, molecular refinements (for example, blue-shifting ChR2 and narrowing the spectrum of VChR1) will probably be required to provide adequate separation at the blue end of the spectrum for certain classes of *in vivo* experiments.

The identification and characterization reported here of VChR1 as a yellow-light photostimulation tool defines the third major functionally distinct category of fast microbial optogenetic tools available for interrogating the organization and function of neural circuits (reviewed in ref. ¹³). The substantially red-shifted action spectrum will allow not only combinatorial control experiments, but also improved integration with existing blue light-activated Ca²⁺ indicators and deeper penetration of light with *in vivo* applications¹⁴ as a result of the reduced scattering of lower-energy photons. The discovery of microbial proteins that can be used as tools for basic science and biotechnology underscores the importance of mining ecological diversity in the cause of neuroscience; there are many opsins with potentially useful properties¹⁵, and this study provides proof of principle for using genomic tools to uncover latent possibilities in microbial genomes.

Supplementary Material

Refer to Web version on PubMed Central for supplementary material.

Acknowledgments

F.Z. is supported by the US National Institutes of Health, F.B. by the Erasmus Program and O.Y. by the European Molecular Biology Organization. K.D. is supported by the California Institute of Regenerative Medicine and the Snyder, Coulter, McKnight and Albert Yu Foundations, as well as by the US National Science Foundation and US National Institutes of Health. P.H. is supported by the Deutsche Forschungsgemeinschaft.

References

1. Zhang F, et al. *Nature* 2007;446:633–639. [PubMed: 17410168]
2. Adamantidis AR, Zhang F, Aravanis AM, Deisseroth K, de Lecea L. *Nature* 2007;450:420–424. [PubMed: 17943086]
3. Nagel G, et al. *Proc Natl Acad Sci USA* 2003;100:13940–13945. [PubMed: 14615590]
4. Boyden ES, Zhang F, Bamberg E, Nagel G, Deisseroth K. *Nat Neurosci* 2005;8:1263–1268. [PubMed: 16116447]
5. Bi A, et al. *Neuron* 2006;50:23–33. [PubMed: 16600853]
6. Li X, et al. *Proc Natl Acad Sci USA* 2005;102:17816–17821. [PubMed: 16306259]
7. Ernst OP, et al. *J Biol Chem* 2008;283:1637–1643. [PubMed: 17993465]
8. Bamann C, Kirsch T, Nagel G, Bamberg E. *J Mol Biol* 2008;375:686–694. [PubMed: 18037436]
9. Nagel G, et al. *Science* 2002;296:2395–2398. [PubMed: 12089443]
10. Hegemann P, Ehlenbeck S, Gradmann D. *Biophys J* 2005;89:3911–3918. [PubMed: 16169986]
11. Kloppmann E, Becker T, Ullmann GM. *Proteins* 2005;61:953–965. [PubMed: 16247786]
12. Hoffmann M, et al. *J Am Chem Soc* 2006;128:10808–10818. [PubMed: 16910676]
13. Gradinaru V, et al. *J Neurosci* 2007;27:14231–14238. [PubMed: 18160630]
14. Aravanis A, et al. *J Neural Eng* 2007;4:S143–S156. [PubMed: 17873414]
15. Venter JC, et al. *Science* 2004;304:66–74. [PubMed: 15001713]

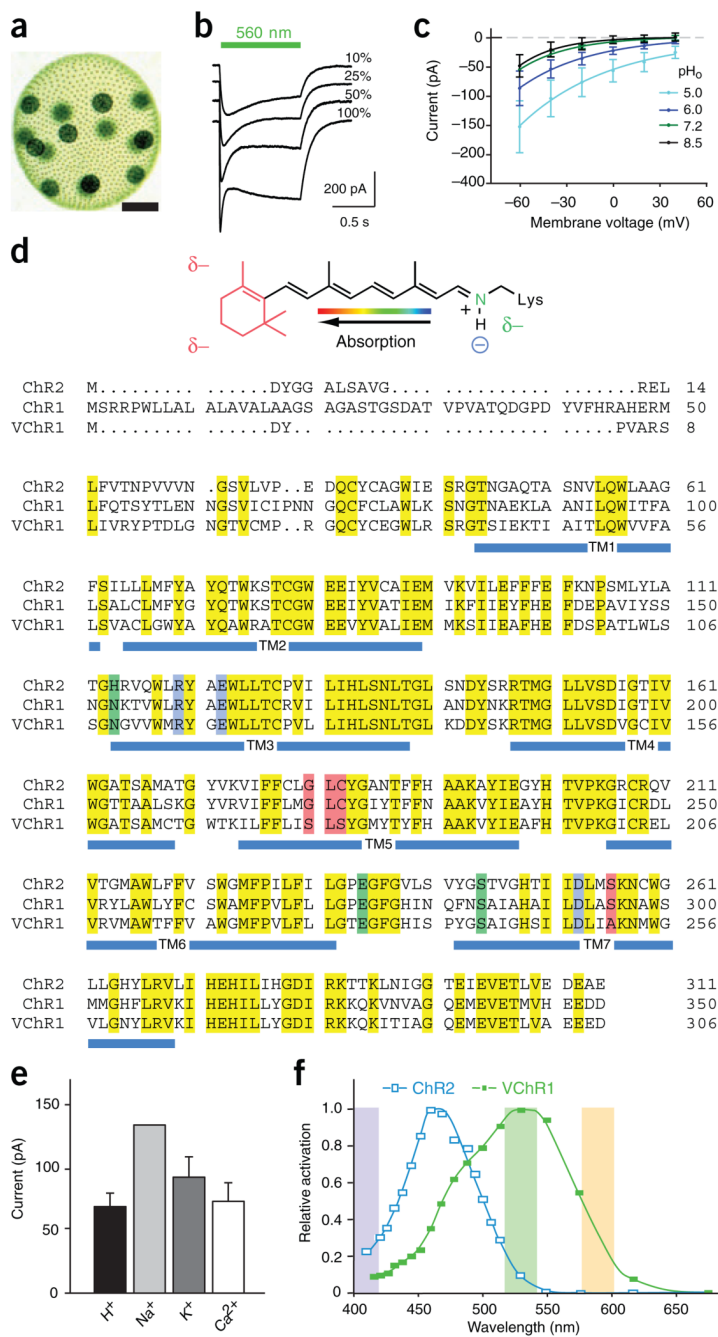
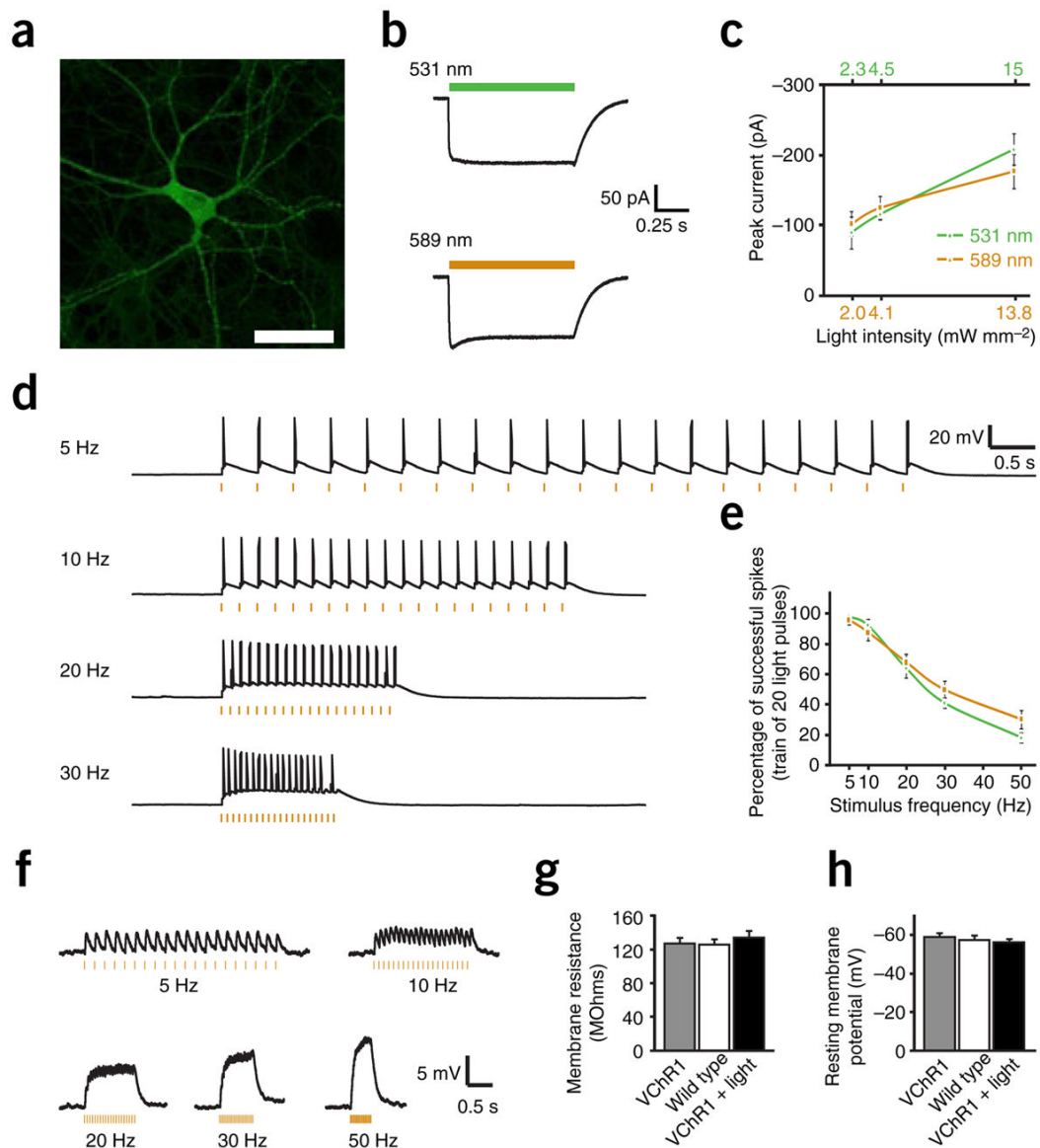


Figure 1. Identification and characterization of VChR1. **(a)** *Volvox carteri* colony showing several thousand small somatic cells and 16 gonidia (scale bar, 125 μm). **(b)** Photocurrents in VChR1-expressing HEK293 cells under varying light intensity (traces represent averages of six recordings). **(c)** *I-V* relationship in HEK293 cells under varying extracellular pH. External and internal [Na⁺] were held constant at 140 mM. **(d)** RSB structure shows the predicted changes in environmental polarity as partial charges (δ⁻; top). Sequence comparison of ChR2, ChR1 and VChR1 is shown with residues highlighted that are predicted to define the RSB Schiff base counterion (blue), modulate electrical potential of the RSB binding pocket (red) or modulate RSB potential via long-range coupling (green). **(e)** Ion flux characteristics of VChR1 in

HEK293 cells ($n = 4$; see Supplementary Methods). **(f)** Action spectra for VChR1 and ChR2 in oocytes; wavelengths used in later figures are shaded. Values are mean \pm s.e.m.

**Figure 2.**

VChR1 permits red-shifted neural photostimulation. **(a)** Cultured hippocampal neuron expressing VChR1-EYFP. A lentiviral vector carrying the α CaMKII promoter was used to drive neuron-specific expression (scale bar, 75 μ m). **(b)** Inward photocurrent in a voltage-clamped VChR1-EYFP neuron evoked by 1 s of 531- or 589-nm light (colored bars). **(c)** Summary data of mean current evoked by 531- or 589-nm light over increasing light intensities ($n = 10$). **(d)** Voltage traces showing spikes in a current-clamped hippocampal neuron evoked by 5-, 10-, 20- or 30-Hz trains of 5-ms light pulses (orange dashes). **(e)** Population data summarizing light-spike fidelity in current-clamped neurons illuminated with 531- or 589-nm light pulses ($n = 12$). **(f)** Barrage summation of subthreshold synaptic-like events evoked with increasing light-pulse frequency. **(g,h)** Membrane resistances and resting membrane potentials of neurons expressing VChR1-EYFP ($n = 10$), not expressing VChR1-EYFP (wild type, $n = 10$), or expressing VChR1-EYFP and measured 24 h after exposure to activating light ($n = 10$). Values are mean \pm s.e.m.

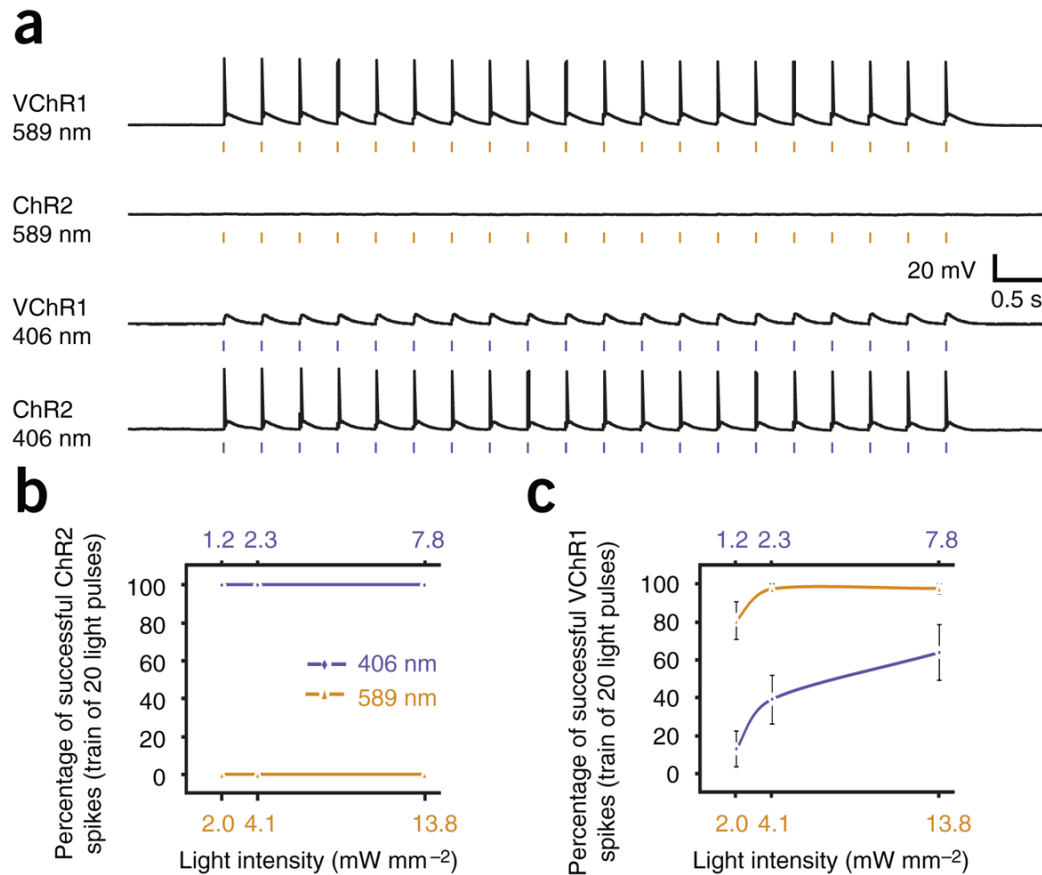


Figure 3. Separable channels of optogenetic excitation. **(a)** Voltage traces showing that ChR2 and VChR1 can be selectively activated by 406- (1.2 mW mm^{-2}) and 589-nm (2.3 mW mm^{-2}) light, respectively. Trains of 5-ms light flashes were delivered at 5 Hz. **(b)** Population data comparing activation of ChR2 by 406- and 589-nm light at three different light intensities ($n = 7$). Trains of 5-ms light pulses were delivered at 5 Hz. **(c)** Population data comparing activation of VChR1 by 406- and 589-nm light at three different light intensities ($n = 10$). Values are mean \pm s.e.m.